MSDE

PAPER

View Article Online
View Journal | View Issue

Cite this: *Mol. Syst. Des. Eng.*, 2021, 6, 627

Zr-MOFs for CF_4/CH_4, CH_4/H_2, and CH_4/N_2 separation: towards the goal of discovering stable and effective adsorbents†

Hakan Demir * and Seda Keskin *

Zirconium metal–organic frameworks (MOFs) can be promising adsorbents for various applications as they are highly stable in different chemical environments. In this work, a collection of Zr-MOFs comprised of more than 100 materials is screened for CF_4/CH_4, CH_4/H_2, and CH_4/N_2 separations using atomistic-level simulations. The top three MOFs for the CF_4/CH_4 separation are identified as PCN-700-BPDC-TPDC, LIFM-90, and BUT-67 exhibiting CF_4/CH_4 adsorption selectivities of 4.8, 4.6, and 4.7, CF_4 working capacities of 2.0, 2.0, and 2.1 mol kg^{-1}, and regenerabilities of 85.1, 84.2, and 75.7%, respectively. For the CH_4/H_2 separation, MOF-812, BUT-67, and BUT-66 are determined to be the top performing MOFs demonstrating CH_4/H_2 selectivities of 61.6, 36.7, and 46.2, CH_4 working capacities of 3.0, 4.1, and 3.4 mol kg^{-1}, and CH_4 regenerabilities of 70.7, 82.7, and 74.7%, respectively. Regarding the CH_4/N_2 separation, BUT-67, Zr-AbBA, and PCN-702 achieving CH_4/N_2 selectivities of 4.5, 3.4, and 3.8, CH_4 working capacities of 3.6, 3.9, and 3.5 mol kg^{-1}, and CH_4 regenerabilities of 81.1, 84.0, and 84.5%, in successive order, show the best overall separation performances. To further elucidate the adsorption in top performing adsorbents, the adsorption sites in these materials are analyzed using radial distribution functions and adsorbate density profiles. Finally, the water affinities of Zr-MOFs are explored to comment on their practical use in real gas separation applications. Our findings may inspire future studies probing the adsorption/separation mechanisms and performances of Zr-MOFs for different gases.

Received 28th May 2021,
Accepted 15th June 2021

DOI: 10.1039/d1me00060h

rsc.li/molecular-engineering

Design, System, Application

In the last two decades, Zr metal–organic frameworks (MOFs) have stood out from the rest of the MOFs as they possess high stability rendering their use in various applications including gas separations. This study employs dozens of Zr-MOFs for the separations of three gas mixtures, CF_4/CH_4, CH_4/H_2, and CH_4/N_2, that should be achieved with high efficiency to mitigate the energy supplied for their separations in industry and diminish their polluting effects on environment. As there is not a single factor determining the gas separation performances, the best Zr-MOFs are determined by considering three metrics, selectivity, working capacity, and regenerability, in conjunction. The structure–property relationships are extracted showing the regions of favorable structural features for high gas separation performances. In addition, for the top performing MOFs, the preferential adsorption sites and local coordination environment of sorbates are demonstrated unraveling highly interacting framework atoms/regions. Since all the materials investigated in this work are experimentally synthesized, these findings may trigger targeted experimental and theoretical works speeding up material discovery efforts for clean energy and environment purposes.

1. Introduction

Metal–organic frameworks (MOFs) are nanoporous, crystalline structures offering tunable chemical environments which can be exploited for various applications including gas storage/separation, catalysis, sensing, drug delivery, *etc.*[1–14] While they possess favorable structural features namely high porosity, ease of functionalization, adjustable pore sizes, *etc.*, many of them suffer from relatively lower thermal, hydrothermal, and/or chemical stability than industrially utilized zeolites.[15–18] Among different subclasses of MOFs, Zr-MOFs have garnered particular interest as some of them have been shown to exhibit good stability at high temperatures, in humid conditions, and/or acidic/basic environments.[19–25] The high stability of Zr-MOFs are attributed to the strong Zr-O bonding, and high connectivity of Zr metals.[20,21,26,27]

Particularly considering gas separation applications for clean energy and environment purposes, so far, many

Department of Chemical and Biological Engineering, Koc University, 34450 Istanbul, Turkey. E-mail: hakdemir@ku.edu.tr, skeskin@ku.edu.tr

† Electronic supplementary information (ESI) available: Ternary plots of the individual separation performance metric contributions; adsorbate density profiles; illustrations of the top Zr-MOFs for the separations discussed; tables listing the gas separation performances of the Zr-MOFs along with their structural features. See DOI: 10.1039/d1me00060h

experimental and theoretical studies using MOFs have been carried out.[28–32] Amongst them, the separation of mixtures involving methane has become one of the most widely investigated areas as the efficient separation/storage of methane can meet some part of the ever-increasing energy need of the societies at affordable cost as well as providing a feedstock for chemical manufacturing. While there are many methane involving gas mixtures found in the industrial premises and the atmosphere, our focus in this study is particularly on the separation of three gas mixtures: CF_4/CH_4, CH_4/H_2, and CH_4/N_2.

Last century witnessed increasing amounts of both CF_4 and CH_4 emissions to the atmosphere as a result of anthropogenic activities whose accumulation in the air create risks for human health and environment.[33–37] Specifically, CF_4 is one of the greenhouse gases that has a much higher global warming potential than the famous greenhouse gas of CO_2 and can stay in the atmosphere for an extended period of time.[34,36,38,39] Although CF_4 can pose health threats when it exists in the open air, it can provide significant economic benefits in several industries. For instance, CF_4 is one of the gases that is employed in the high value-added industry of semiconductor fabrication due to its non-corrosive, non-flammable and stable nature.[38,40] Similar to CF_4, CH_4 has a higher global warming potential[41] than CO_2 whose emission to the atmosphere leads to not only environmental pollution but also a great economic loss as methane is increasingly being used for various purposes including transportation, heating, value-added chemical production, *etc.*[7,41–43] Therefore, efficient separation of the CF_4/CH_4 mixture present in the air would not only make more CH_4 available for energy and chemical feedstock needs but also can present a fresh source of CF_4 which could lower the semiconductor manufacturing costs. Senkovska *et al.*[36] explored the CF_4 storage in several MOFs at room temperature and pressure and found out that their CF_4 uptake amounts are about 0.4–1.9 mmol g^{-1}. Calero *et al.*[44] predicted that Cu-BTC adsorb ~1 (4) mol kg^{-1} of CF_4 at 1 (10) bar, 300 K using molecular simulations.

One of the most common gas mixtures that can be found in the industry is CH_4/H_2 mixture due to the ubiquitously employed methane steam reforming and methane dry reforming processes.[45,46] Since both CH_4 and H_2 can be used in vehicular fuel cells, achieving their efficient separation can help accelerate the transition to cleaner energy sources.[45,47] Altintas *et al.*[48] studied CH_4/H_2 separation in hundreds of MOFs where the CH_4/H_2 adsorption selectivities, CH_4 working capacities, and regenerabilities are reported to vary roughly in the ranges of $10^{-2} - 5 \times 10^2$, $10^{-2} - 6$ mol kg^{-1}, and 15–100% for an equimolar CH_4/H_2 mixture at 10 bar, 298 K. Another study[49] showed that the CH_4/H_2 adsorption selectivities of the top MOF membranes identified are in the range of 8.31–97.36 for an equimolar CH_4/H_2 mixture at 1 bar, 298 K. Liu *et al.*[50] probed the CH_4/H_2 separation performances of IRMOFs (isoreticular MOFs) using grand canonical Monte Carlo (GCMC) simulations revealing their CH_4/H_2 selectivities at 10 bar, 298 K to be around 5–20 for equimolar CH_4/H_2 mixtures. Wu *et al.*[46] examined a selected list of MOFs unveiling their CH_4/H_2 adsorption selectivities to be in the range of 50.60–126.07 for an equimolar mixture at 10 bar, 298 K.

CH_4 and N_2 can co-exist in natural gas,[51] landfill gas,[52] coal mine methane.[53,54] The separation of CH_4 from N_2 is not a trivial task as both gases have similar molecular sizes.[51] Sumer *et al.*'s computational investigation[52] on MOFs revealed that the top performing MOFs exhibit CH_4/N_2 adsorption selectivities of 4.58–6.71, CH_4 working capacities of 2.55–3.69 mol kg^{-1}, and regenerabilities of 75.4–80.1% for an equimolar CH_4/N_2 mixture at 298 K, 10 bar. Li *et al.*[54] investigated the CH_4/N_2 separation in a Co-based MOF and predicted the CH_4/N_2 adsorption selectivity to range between 8.5 and 12.5 at ambient conditions using Ideal Adsorbed Solution Theory (IAST).[55] Qiao *et al.*[56] estimated the ideal N_2/CH_4 selectivities of thousands of MOFs at 298 K which vary from 3×10^{-2} to 10. Kim *et al.*[57] studied a series of functionalized UiO-66 structures for the separation of an equimolar CH_4/N_2 mixture at 1 bar, 298 K and determined that UiO-66-Br_2 exhibits the largest CH_4/N_2 selectivity of 5.1. Liu *et al.*[58] estimated the CH_4/N_2 selectivities of a Co and Ni based MOF (Co- and Ni-MA-BPY) to be 7.2 and 7.4 using IAST for an equimolar CH_4/N_2 mixture at ambient conditions. In the preceding studies, the gas separation performances of the materials are evaluated using mostly one or two metrics, generally using selectivity, which could be insufficient in determining the top materials. Besides, in many of such studies, the strongest adsorption sites in the top materials are not shown. As such aspects are crucial for the design and use of materials, our objective is to assess materials' gas separation performances holistically and determine the favorable adsorption sites in the selected top materials.

Herein, we explore the separation performances of Zr-MOFs for the CF_4/CH_4, CH_4/H_2, and CH_4/N_2 mixtures by mimicking vacuum swing adsorption (VSA) and pressure swing adsorption (PSA) conditions at room temperature. Considering the trade-offs between multiple separation performance metrics, MOFs are ranked by taking into account adsorption selectivity, working capacity, and regenerability. The adsorption sites of the top MOFs are analyzed using sorbate density profiles and radial distribution functions (RDFs). The analysis of the CH_4/N_2 separation performances is done using PACMOF[59] (partial atomic charges in metal–organic frameworks) and EQeq[60] (extended charge equilibration) charges to find out the extent of influence of two charge partitioning methods on separation performances. Finally, the water affinities of the MOFs are assessed by computing the Henry's constant and heat of adsorption of water at infinite dilution at the room temperature. Our results will contribute to accelerating the experimental and theoretical quest of finding synthesized, and stable structures whose use in the preceding separations can present economic and environmental benefits.

2. Computational methods

Zr-MOF structures are based on the work of Zhou *et al.*[61] from which only those without open metal sites and partial occupancies are kept. For each gas mixture, the list of Zr-MOFs is further narrowed down by selecting the structures with pore limiting diameters (PLDs) larger than each sorbate. The gas uptakes and selectivities are attained through GCMC simulations for which 10 000 (10 000), 10 000 (10 000), and 25 000 (25 000) equilibration (production) cycles are employed at 298 K for equimolar CF_4/CH_4, CH_4/H_2 and CH_4/N_2 mixtures, successively, in RASPA.[62] The adsorption and desorption pressures are 1 and 0.1 bar for CF_4/CH_4 separation, 10 and 1 for CH_4/H_2 separation, and 10 and 1 bar for CH_4/N_2 separation, respectively. The gas molecules are allowed to have insertion/deletion, translation, rotation (for N_2), and identity change moves with equal probabilities. CF_4 molecule is represented as a single site based on the work of Skoulidas *et al.*[63] Both CH_4 and N_2 molecules are defined by TraPPE models,[64,65] whilst H_2 parameters are obtained from Buch *et al.*[66] MOF interaction parameters are acquired from UFF.[67] Lennard-Jones interactions are cutoff at 12 Å. MOF atoms are assigned PACMOF and EQeq charges separately to test the sensitivity of the results to the charge assignment method. Electrostatic interactions are determined using Ewald summation.[68] The pore analysis, determining structural features (*i.e.*, probe-occupiable pore volume), is done using Zeo++[69] where a probe radius of 1.84 Å (when applicable) is employed. The identification and blocking of the inaccessible regions is performed by the insertion of spheres with radii slightly lower (0.1 Å) than the molecular radii of respective gases considering structural flexibility. The gas separation performances of the MOFs are evaluated through three metrics, adsorption selectivity, working capacity, and regenerability, which are used in combination to rank the materials.

The adsorption selectivity of the first gas species over the second gas is defined as $S_{ads,1/2} = \frac{N_1/N_2}{y_1/y_2}$ where N and y denote the gas loading in the structure and mole fraction of the gas component in the mixture, respectively. Working capacity is calculated as the difference of gas uptakes at adsorption and desorption pressures, $\Delta N_1 = N_{ads,1} - N_{des,1}$. Regenerabilities of the materials are determined using $R = \frac{\Delta N_1}{N_{ads,1}}$. The Henry's constants and heats of adsorption of H_2O at infinite dilution in the MOFs are determined by employing 10 000 000 Widom insertions at 298 K. Structures whose Henry's constants of H_2O deviate considerably (*i.e.*, >50%) are not included. It has been shown earlier that the usage of generic force fields for high-throughput screening purposes, which our work is based on, can be qualitatively accurate in determining the gas interaction trends, and/or the top performing structures regarding various gas adsorption/separation applications.[70–73] Specifically, Yang *et al.*[74] has previously shown that the experimental and simulated CH_4 adsorption uptakes (obtained using UFF) in UiO-66 based Zr-MOFs are in accord with each other. However, it should also be cautioned that due to various reasons including but not limited to incomplete sample activation, presence of defect in materials, deficiencies of force fields, there can be discrepancies between experimental and simulated adsorption/separation performances.

3. Results & discussion

The selected Zr-MOFs are screened for the CF_4/CH_4, CH_4/H_2, and CH_4/N_2 separations using GCMC simulations to extract their relevant separation performance metrics and rank them by considering all three performance metrics. Starting with CF_4/CH_4 separation, the following discussion details the pathway towards identifying the best materials and the investigation of the adsorption sites of the top materials identified for each gas separation. As the water stability of the MOFs is another significant factor to take into account for practical use, the water affinities of the structures are also discussed towards the end of the section. It should be noted that a recent study demonstrates the structural disparities in databases can result in considerably different gas uptakes, selectivities, and material rankings in material screening studies implying the necessity of highly accurate structures for accurate predictions.[31] These disparities may arise due to multiple reasons including lack of optimization, missing atoms, structural disorders, *etc.* Our study focuses on refined, optimized Zr-MOFs some of which (*e.g.*, QAJJOD, QAJPEZ, ISENAX *etc.*) are reported with disorders and/or missing atoms in other databases such as Cambridge Structural Database (CSD) and/or CoRE MOF or not reported at all. Due to the existence of higher quality structures some of which are not available in other databases, in this study, it is anticipated to have more accurate and comprehensive predictions than those relying on fewer number of Zr-MOFs and/or Zr-MOFs with no refinement or lower level of refinements.

Fig. 1 delineates the correlations between the CF_4/CH_4 adsorption selectivities of the Zr-MOFs and their CF_4 working capacities, CF_4 regenerabilities, PLDs, surface areas, and void fractions. The ranges of CF_4/CH_4 adsorption selectivity, CF_4 working capacity, and CF_4 regenerability of all Zr-MOFs are 0.8–6.2, 0.3–2.1 mol kg^{-1}, and 54.0–89.9%, successively. Examining the top left panel, it can be inferred that for the majority of the MOFs there is a linear relationship between S_{CF_4/CH_4} and ΔN_{CF_4}. BUT-66, the most CF_4 selective MOF (S_{CF_4/CH_4} = 6.2), is an exception to this observation which demonstrates a mediocre CF_4 working capacity of 1.3 mol kg^{-1}. Another discernible aspect of this MOF is its low CF_4 regenerability of 54% which is the lowest among all Zr-MOFs while most of the MOFs are highly regenerable ($R_{CF_4} > 80\%$). In contrast, there are two almost unselective Zr-MOFs which possess low ΔN_{CF_4} values (<0.5 mol kg^{-1}).

The top right panel shows that the most CF_4 selective Zr-MOF and that with the highest CF_4 working capacity (BUT-66

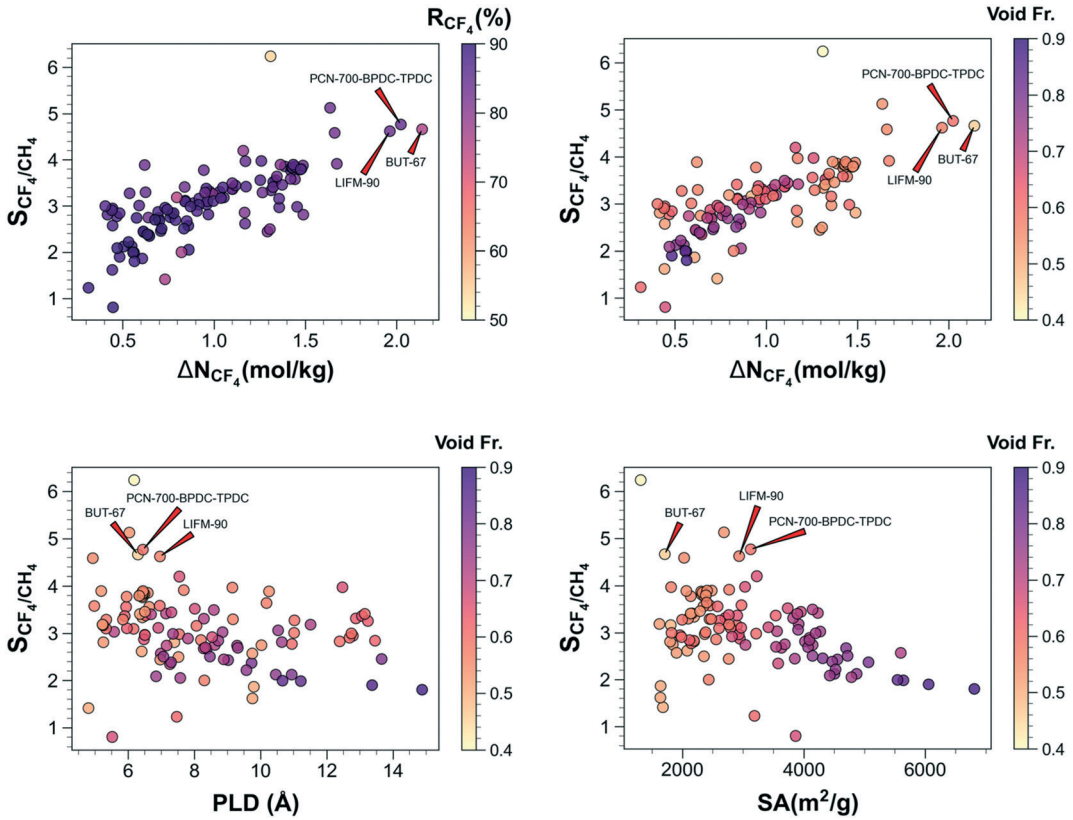

Fig. 1 CF_4/CH_4 adsorption selectivities of the Zr-MOFs with respect to two other metrics and structural features.

and BUT-67) possess low void fractions of 0.406 and 0.461, respectively. Conversely, highly porous Zr-MOFs (void fractions $>$ 0.75) mostly attain relatively low CF_4/CH_4 selectivities (1.8–3.1). Those with medium void fractions (0.4 $<$ void fraction $<$ 0.7) are scattered throughout the entire CF_4 working capacity and CF_4/CH_4 selectivity spectra. The bottom left panel portrays the relationship between the CF_4/CH_4 selectivity and PLD of the Zr-MOFs which depicts that the most CF_4 selective MOFs have narrow PLD sizes. Yet, a small PLD does not necessarily translate to high CF_4/CH_4 selectivity which can be exemplified by MOF-805, with the smallest PLD size of 4.8 Å, showing one of the lowest CF_4/CH_4 selectivities of 1.4. The bottom right panel describes the change of CF_4/CH_4 selectivity with respect to the surface areas of the structures where the selectivities drop as the surface areas expand. It can be seen that the most CF_4 selective MOF, BUT-66, bears the lowest surface area of 1311.7 m^2 g^{-1}. PCN-230 with the largest surface area of 6807.5 m^2 g^{-1} demonstrates a low CF_4/CH_4 selectivity of 1.8 while lower CF_4/CH_4 selectivities are attained by several other MOFs.

Considering the results presented so far, it can be inferred that there can be substantial trade-offs across different separation performance metrics of the materials. Therefore, a material ranking solely based on a single separation performance metric could be misleading given multiple factors affect the overall separation performance of the materials. In this work, the material separation performances of Zr-MOFs are assessed based on the overall separation performance scores which are basically summation of individual performance scores, $\text{Score}_{X,i} = \frac{X_i}{X_{\text{Max}}} \times 100$. Here, X_i, and X_{Max} stand for the predicted value of the performance metric X for the material i, and the highest predicted value of the performance metric X across all Zr-MOFs, respectively.

Table 1 enlists the CF_4/CH_4 separation performance metrics and structural features of the top 10 Zr-MOFs determined using the overall separation performance scores (*i.e.*, summation of adsorption selectivity score, working capacity score, and regenerability score). The CF_4/CH_4 adsorption selectivity, CF_4 working capacity, and CF_4 regenerability ranges are 3.8–5.1, 1.5–2.1 mol kg^{-1}, and 75.7–86.3% indicating that CF_4/CH_4 separation performances of the top materials are similar. These top-performing MOFs possess PLDs of 4.93–7.68 Å, surface areas of 1708.7–3122.9 m^2 g^{-1}, void fractions of 0.461–0.602, and pore volumes of 0.501–0.800 cm^3 g^{-1}. Among them, PCN-700-BPDC-TPDC, LIFM-90, and BUT-67 exhibit the best overall separation performances with selectivities of 4.8, 4.6, and 4.7, CF_4 working capacities of 2.0, 2.0, and 2.1 mol kg^{-1}, and regenerabilities of 85.1, 84.2, and 75.7%, successively. The first two MOFs have similar porous features (*i.e.*, PLDs, surface areas, void fractions, pore volumes) while the third MOF is comparatively less porous and has smaller pores.

Table 1 Separation performance metrics and structural information regarding the 10 top-performing Zr-MOFs for the separation of CF_4/CH_4 gas mixture

Structure	SCF_4/CH_4	ΔN_{CF_4} (mol kg^{-1})	R_{CF_4} (%)	GCD (Å)	PLD (Å)	LCD (Å)	SA (m^2 g^{-1})	V_f	V_p (cm^3 g^{-1})
PCN-700-BPDC-TPDC	4.8	2.0	85.1	8.71	6.44	8.71	3122.9	0.602	0.800
LIFM-90	4.6	2.0	84.2	7.97	6.96	7.97	2933.4	0.576	0.737
BUT-67	4.7	2.1	75.7	7.96	6.29	7.90	1708.7	0.461	0.501
PU-1	5.1	1.6	83.4	10.92	6.03	10.92	2683.6	0.543	0.753
BUT-11	4.6	1.7	82.9	10.25	4.93	10.25	2026.8	0.558	0.616
PCN-700-NDC-BDDC	3.9	1.7	83.2	8.45	7.68	8.45	2768.5	0.577	0.736
LIFM-78	3.9	1.5	85.1	7.02	6.43	7.00	2307.9	0.555	0.613
LIFM-76	3.8	1.5	85.9	6.94	6.36	6.94	2317.5	0.543	0.599
LIFM-83	3.8	1.5	86.3	7.05	6.33	7.05	2385.2	0.548	0.609
LIFM-77	3.8	1.5	86.1	6.99	6.42	6.99	2353.3	0.546	0.602

GCD: global cavity diameter, PLD: pore limiting diameter, LCD: largest cavity diameter, SA: surface area, V_f: void fraction, V_p: pore volume.

Fig. 2 illustrates a ternary plot describing the contribution of each separation performance metric to the overall separation performance score (circles scaled with respect to the overall separation performance score). If all three separation performance metrics were to contribute equally, the materials would lie at the center of the triangle. Considering this interpretation, it can be deduced that for the top 10 materials (denoted as blue circles), the contributions of separation performance metrics are comparable while for many of the rest of the materials (shown as red circles), regenerability scores can have higher contribution to the overall separation performance score. This signifies that there can be cases where regenerability of the materials can change the overall ranking of the materials. For instance, BUT-66, ranked 17th using the overall separation performance score as defined above, would have a ranking of 4th if it was ranked based on the summation of only CF_4/CH_4 adsorption selectivity and CF_4 working capacity scores. This finding underscores the need of considering multiple separation performance metrics (including regenerability) in determining the final material shortlists for further studies.

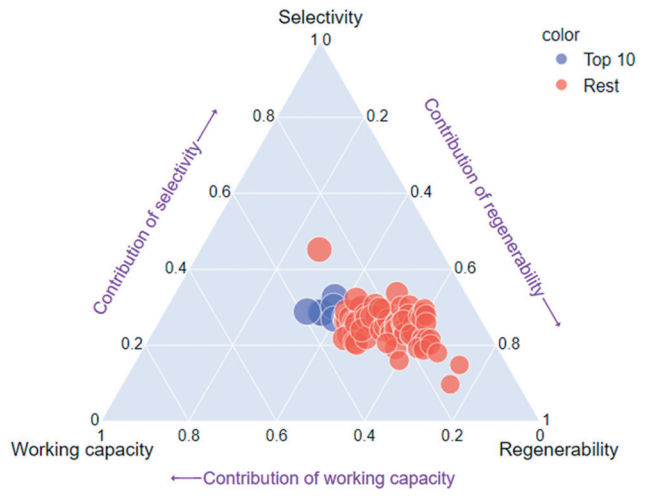

Fig. 2 Ternary plot of CF_4/CH_4 separation performance metrics showing their contributions to overall separation performance score.

To better understand the adsorption mechanisms and find out the underlying reasons behind the top separation performances, the elucidation of the adsorption sites and local environments of the adsorbates is crucial. Fig. 3 demonstrates the CF_4 density profiles in the top three Zr-MOFs (PCN-700-BPDC-TPDC, LIFM-90, and BUT-67) at the desorption and adsorption conditions. In both conditions, for the first two materials, despite some low adsorption probability near the metal nodes CF_4 generally prefers to adsorb near the center of the linker, away from the metal nodes while in the third best MOF it adsorbs in the pocket between two metal nodes where they stay closer to H and C atoms of the framework. Fig. 3 also portrays the CH_4 density profiles in the same three Zr-MOFs at both desorption and adsorption conditions where it can be seen that CH_4 adsorption profile has similarities with that of CF_4 in PCN-700-BPDC-TPDC and LIFM-90 albeit pronounced adsorption closer to metal nodes, especially at the adsorption conditions. In BUT-67, CH_4 tends to adsorb near the intersection of linker and metal node in the large pore while still being closer to the organic moieties.

Fig. 4 exhibits the normalized RDF plots of both adsorbates at the adsorption conditions. As expected, the similarities observed in the sorbate density profiles of PCN-700-BPDC-TPDC and LIFM-90 are carried over to the RDF plots. For instance, in both materials, RDF plots indicate that CF_4 and CH_4 are located much closer to the organic parts than the metals (~4–5 Å *vs.* ~6–7 Å) with similar local environments. In contrast, in BUT-67, CF_4 and CH_4 show discrepancies in their RDFs as they adsorb at different sites. For example, the probability of finding a framework O atom near CH_4 (around 5 Å) is higher than CF_4 which is an indication of different siting of adsorbates in the porous network. Yet, Zr atom remains to be the farthest atom to the sorbates in BUT-67 as they are shielded by O atoms. Overall, these observations imply that different adsorption amounts of CF_4 and CH_4 (thus, selective behaviors of the MOFs) are engendered by disparate interaction strengths between the sorbates and adsorption sites which, in turn, leads to differing adsorbate occupancies. Specifically in BUT-67, the larger sorbate, CF_4, strongly prefers a narrow pocket (~4.5 Å,

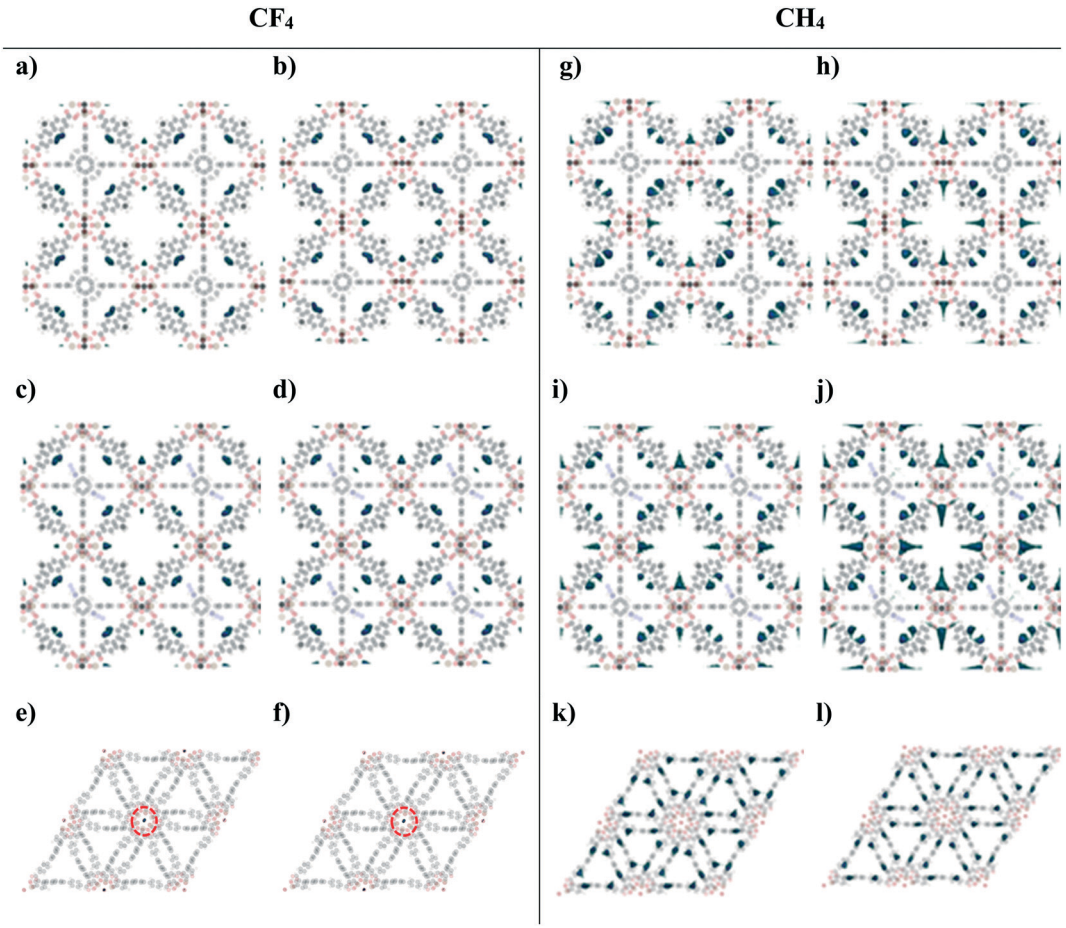

Fig. 3 (Left panel) CF_4 density profiles in PCN-700-BPDC-TPDC (a and b), LIFM-90 (c and d), and BUT-67 (e and f) at 0.1 (left) and 1 (right) bar at 298 K. (Red circles denoting adsorption sites at the center of BUT-67) (right panel) CH_4 density profiles in PCN-700-BPDC-TPDC (g and h), LIFM-90 (i and j), and BUT-67 (k and l) at 0.1 (left) and 1 (right) bar at 298 K.

estimated by Platon[75,76]) between the nodes whereas CH_4 adsorbs in the larger pores (>6 Å) where dispersion effects are smaller. As the employed method to identify inaccessible pores did not identify the pocket between metal nodes to be inaccessible for CF_4, this should be deemed as a theoretical gate opening/closing case where it is assumed that the flexibility effects would allow CF_4 adsorption but prevent CH_4 adsorption. This prediction suggests that the design of adsorbents with small pockets can be useful in separating nonpolar species with high selectivity factors. However, this design strategy could be of less use for membranes as very narrow pores can hamper the diffusion of sorbates.

Fig. 5 manifests the CH_4/H_2 separation performance metrics in tandem with structural properties of the Zr-MOFs. The separation performance metrics (*i.e.*, CH_4/H_2 adsorption selectivity, CH_4 working capacity, and CH_4 regenerability) span the ranges of 3.0–61.6, 0.8–4.1 mol kg^{-1}, and 70.7–89.7%, respectively. The top left panel indicates that most of the Zr-MOFs have fairly high CH_4 regenerabilities (larger than 85%) while the three most CH_4 selective (over H_2) Zr-MOFs (MOF-812, BUT-66, and Zr-DTDC) possess comparatively lower CH_4 regenerabilities (70.7–75.1%). For instance, the most CH_4 selective (over H_2) Zr-MOF, MOF-812, exhibits a CH_4 regenerability of 70.7% along with a CH_4 working capacity of 3.0 mol kg^{-1}. In contrast, the Zr-MOF with the largest CH_4 working capacity of 4.1 mol kg^{-1}, Zr-AbBA, attains a high CH_4 regenerability of 84.8%. The top right panel shows that, in general, as the structures possess higher void fractions, they tend to be less selective towards CH_4 for which PCN-230 (void fraction of 0.877) can be an example with a CH_4/H_2 selectivity of 3.0. The top three MOFs in terms of CH_4/H_2 adsorption selectivity have lower void fractions (0.345–0.449) than many other Zr-MOFs investigated. This can be one of the reasons for having relatively smaller CH_4 regenerabilities in these structures. Not surprisingly, Zr-AbBA with the largest CH_4 working capacity possesses a large void fraction of 0.639 and pore volume of 1.094 $cm^3\ g^{-1}$.

The bottom left panel demonstrates the inverse relation between the CH_4/H_2 adsorption selectivity and PLDs where the lowest adsorption selectivity is attained by PCN-230, having the highest PLD of 14.88 Å. In contrast, the most CH_4 selective (over H_2) MOF, MOF-812, has one of the smallest PLDs of 3.97 Å. One important observation is that in the small PLD spectrum, there are also MOFs which can exhibit medium CH_4/H_2 selectivities implying that selectivity is not solely a function of PLDs. For instance, UiO-66-NH_2 with the

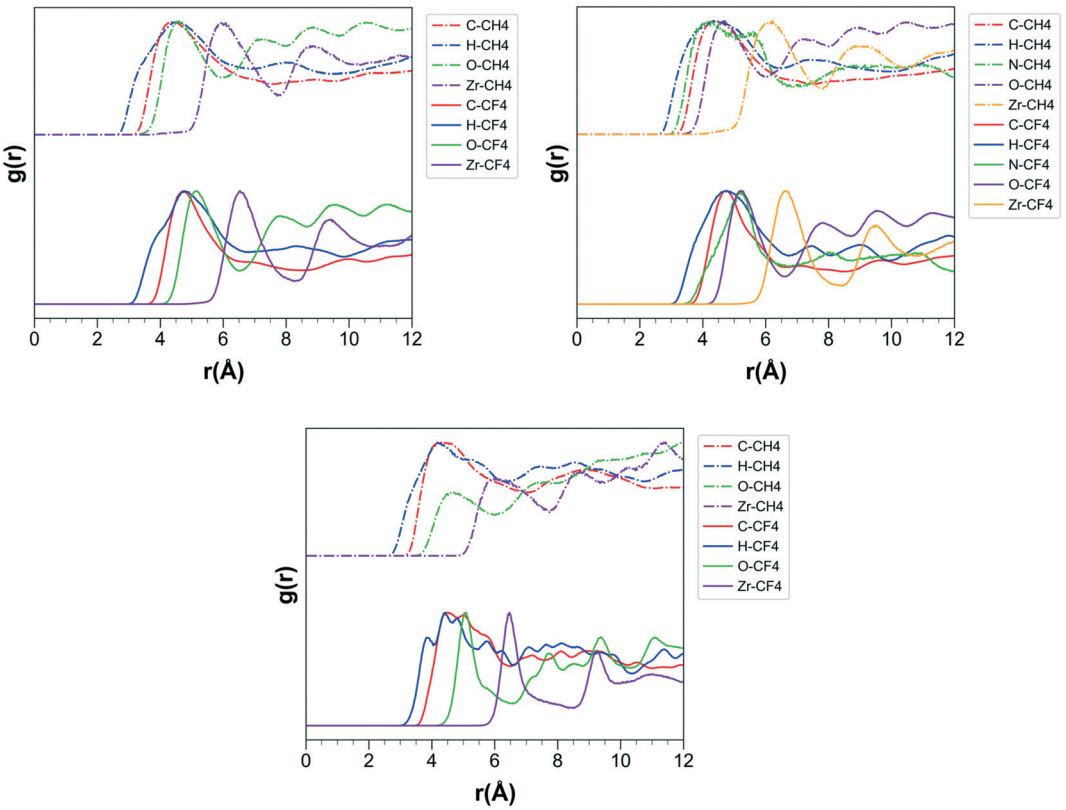

Fig. 4 Normalized RDF plots of the sorbates for the CF_4/CH_4 mixture at 1 bar, 298 K in PCN-700-BPDC-TPDC (left), LIFM-90 (right), and BUT-67 (bottom).

smallest PLD of 3.80 Å can achieve a mediocre CH_4/H_2 selectivity of 11.3 which is roughly one fifth of the highest CH_4/H_2 selectivity that is observed in Zr-MOFs. The drastic reduction of CH_4/H_2 selectivities with the surface areas of the MOFs is illustrated in the bottom right panel where it can be seen that the least CH_4 selective (over H_2) material, PCN-230, does not only have the largest PLD but also have the largest surface area of 6807.5 $m^2\ g^{-1}$. Contrarily, the most CH_4 selective (over H_2) MOF has a relatively low surface area of 939.8 $m^2\ g^{-1}$ which is one of the limiting factors for the CH_4 working capacity.

Table 2 shows the 10 best Zr-MOFs for the CH_4/H_2 separation as determined by the overall separation performance score which possess PLDs of 3.97–7.54 Å, surface areas of 939.8–3213.6 $m^2\ g^{-1}$, void fraction of 0.345–0.612, and pore volumes of 0.294–0.813 $cm^3\ g^{-1}$ demonstrating the CH_4/H_2 adsorption selectivities of 19.4–61.6, CH_4 working capacities of 3.0–4.1 mol kg^{-1}, and CH_4 regenerabilities of 70.7–85.2%. Amongst them, MOF-812, BUT-67, and BUT-66 are identified to be the top three MOFs with the CH_4/H_2 selectivities of 61.6, 36.7, and 46.2, CH_4 working capacities of 3.0, 4.1, and 3.4 mol kg^{-1}, and CH_4 regenerabilities of 70.7, 82.7, and 74.7%, successively. The top material for the CH_4/H_2 separation, MOF-812, is considerably less porous than the second and third ranked MOFs as MOF-812 has a narrow PLD of 3.97 Å, low surface area of 939.8 $m^2\ g^{-1}$, a small void fraction of 0.345 and pore volume of 0.294 $cm^3\ g^{-1}$, whereas BUT-67 and BUT-66 possess larger PLDs of 6.29 and 6.18 Å, surface areas of 1708.7 and 1311.7 $m^2\ g^{-1}$, void fractions of 0.461 and 0.406, and pore volumes of 0.501 and 0.387 $cm^3\ g^{-1}$, successively.

Fig. S1† is a visual description of the contribution of each CH_4/H_2 separation performance metric to the overall separation performance score where it can be seen that for the top 10 materials, the contributions for the top 10 materials are relatively more balanced than those for the rest of the materials, where regenerability (selectivity) scores can have higher (lower) effect. Given the high CH_4 regenerabilities of Zr-MOFs, this implies that many MOFs outside the top 10 list may not achieve CH_4/H_2 selectivities and CH_4 working capacities near the maximum CH_4/H_2 selectivity and CH_4 working capacity.

Fig. S2† depicts the CH_4 density profiles in the top three MOFs for the CH_4/H_2 separation at desorption and adsorption conditions. In MOF-812, CH_4 molecules preferentially adsorb near H and C atoms of the framework which are also relatively close to the O atoms of the metal nodes as the pores are narrow. In BUT-67 and BUT-66, the preferential CH_4 adsorption sites form a hexagonal shape as CH_4 molecules adsorb near the linkers relatively close to the metal nodes. As the pressure is increased from desorption (1 bar) to adsorption pressure (10 bar), while these adsorption sites in the top three MOFs remain to be the most important sites, additional adsorption sites start to emerge in MOF-812

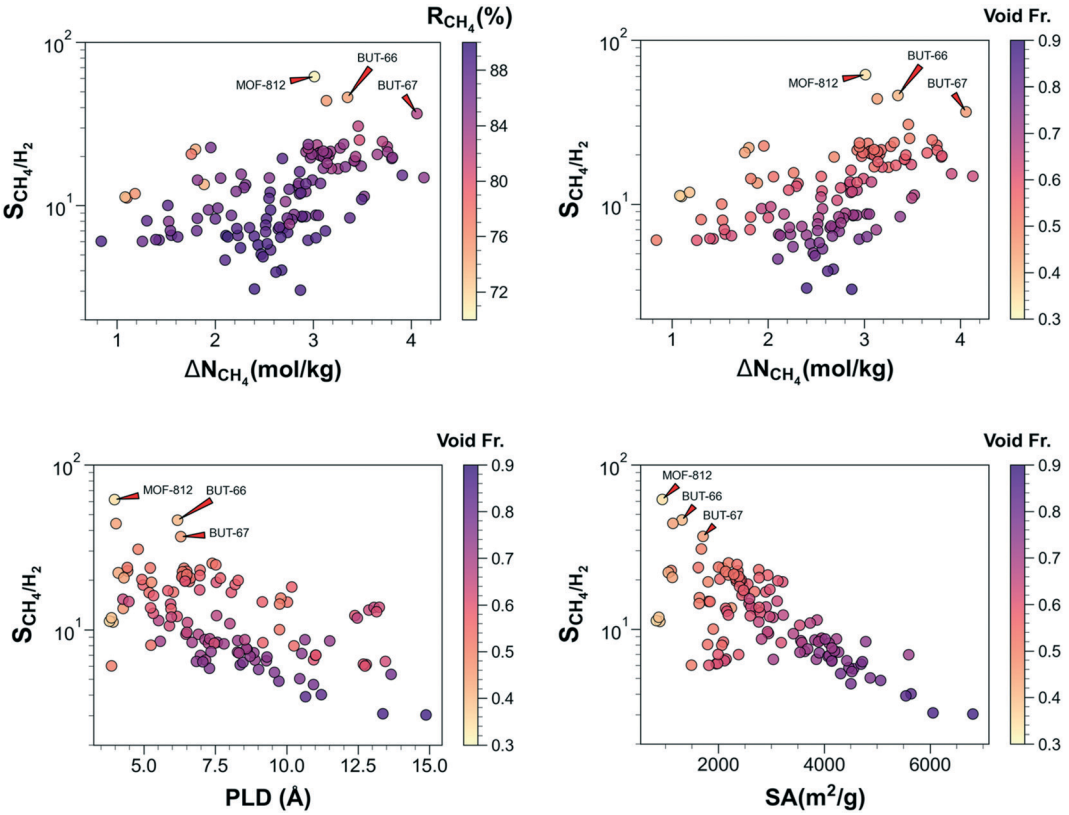

Fig. 5 CH_4/H_2 adsorption selectivities of the Zr-MOFs at 298 K along with CH_4 working capacity, CH_4 regenerability, and porous characteristics of them.

Table 2 Separation performance metrics of the 10 top-performing Zr-MOFs for the separation of CH_4/H_2 gas mixture

Structure	S_{CH_4/H_2}	ΔN_{CH_4} (mol kg^{-1})	R_{CH_4} (%)	GCD (Å)	PLD (Å)	LCD (Å)	SA (m^2 g^{-1})	V_f	V_p (cm^3 g^{-1})
MOF-812	61.6	3.0	70.7	5.80	3.97	5.79	939.8	0.345	0.294
BUT-67	36.7	4.1	82.7	7.96	6.29	7.90	1708.7	0.461	0.501
BUT-66	46.2	3.4	74.7	6.98	6.18	6.98	1311.7	0.406	0.387
Zr-DTDC	44.0	3.1	75.1	8.42	4.02	8.42	1140.1	0.449	0.382
MOF-805	30.7	3.5	82.0	9.23	4.80	9.23	1677.5	0.507	0.489
PCN-700-BDC-BDDC	24.7	3.7	82.2	8.84	7.52	8.84	2353.2	0.542	0.642
LIFM-92	23.0	3.8	83.0	7.97	6.97	7.97	2761.6	0.550	0.689
LIFM-90	21.3	3.8	84.2	7.97	6.96	7.97	2933.4	0.576	0.737
PCN-700-BPDC-TPDC	19.7	3.8	85.1	8.71	6.44	8.71	3122.9	0.602	0.800
PCN-702	19.4	3.8	85.2	8.76	7.54	8.20	3213.6	0.612	0.813

GCD: global cavity diameter, PLD: pore limiting diameter, LCD: largest cavity diameter, SA: surface area, V_f: void fraction, V_p: pore volume.

in its small pores. Fig. S3† represents the H_2 adsorption sites in the top three MOFs for the CH_4/H_2 separation at the desorption and adsorption conditions. In MOF-812, H_2 molecules are located near the benzene groups of the linker as CH_4 molecules are. However, in the case of H_2, molecules are also distributed towards the center of the pores, especially at the adsorption conditions. In BUT-67 and BUT-66, the primary H_2 adsorption sites near the linkers are accompanied with the secondary adsorption sites towards the pore centers as it can be observed at the desorption conditions. At the adsorption conditions, in these two materials, both the primary and secondary adsorption sites are occupied at comparable extents.

Fig. 6 delineates the normalized RDF plots of the CH_4 and H_2 at the adsorption conditions in the top three MOFs identified. In MOF-812, both sorbates are likely to be found near the H and C atoms of the framework whereas O atoms of the framework are slightly farther away from the sorbates which surround the Zr atoms. In BUT-67 and BUT-66, CH_4 and H_2 molecules prefer positions near H and C atoms of the framework as well, but O atoms of the framework are less likely to be found near the sorbates at close distances. While RDF plots provide similar trends for both sorbates, a crucial difference about the local environments of the sorbates can be observed once these RDF plots are considered together with the density plots. Fig. S3† shows that especially at 10

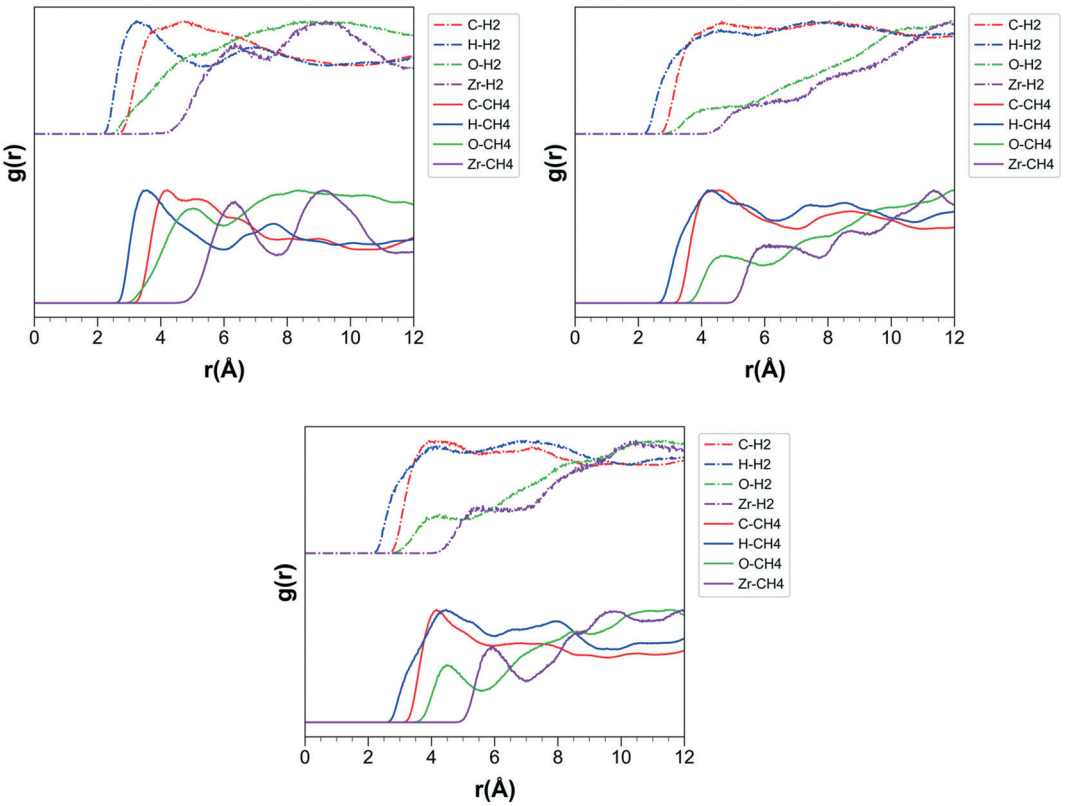

Fig. 6 Normalized RDF plots of the sorbates at 10 bar, 298 K determined for the CH_4/H_2 mixture in MOF-812 (left), BUT-67 (right), and BUT-66 (bottom).

bar, H_2 favors the pore centers due to the attraction forces between adsorbed molecules whereas CH_4 remains to favor the pore walls. This hints that materials with shorter linkers, thus smaller pores, can prevent H_2 building up around the pore centers improving CH_4/H_2 selectivity.

Fig. 7 illustrates the correlations between the CH_4/N_2 separation performance metrics (calculated using PACMOF charges) as well as the relations between the CH_4/N_2 adsorption selectivity and structural features. The investigated Zr-MOFs are found to demonstrate CH_4/N_2 selectivities of 1.5–6.3, CH_4 working capacities of 0.8–3.9 mol kg^{-1}, and CH_4 regenerabilities of 68.9–89.6%. The top left panel shows that most of the MOFs are highly CH_4 regenerable (>80%) while the three most CH_4 selective MOFs are comparatively less regenerable (68.9–73.7%). These MOFs have relatively high CH_4 working capacities (2.6, 2.8, and 2.9 mol kg^{-1}), however, there are many other MOFs that can outperform them in this regard. For instance, Zr-AbBA shows the largest CH_4 working capacity of 3.9 mol kg^{-1} which also exhibits a fairly high CH_4 regenerability of 84.0%. However, its CH_4/N_2 selectivity (3.4) is about half of the maximum selectivity observed.

The top right panel demonstrates that Zr-MOFs with high void fractions have smaller CH_4/N_2 selectivities than less porous Zr-MOFs. For instance, while PCN-230 with the largest void fraction of 0.877 possesses a low CH_4/N_2 selectivity of 1.7, MOF-812 with the smallest void fraction of 0.345 attains the highest CH_4/N_2 selectivity of 6.3. Although there is a general trend of finding MOFs with higher void fractions around medium, high CH_4 working capacity values, the correlation between void fraction and CH_4 working capacity is not straightforward as MOFs with low void fractions are scattered throughout almost the entire CH_4 working capacity spectrum. Comparing the top panels, it can be deduced that having high void fractions help achieving high CH_4 regenerabilities. Due to the confinement effects, it can be expected that MOFs with small pore sizes would be highly selective. In the bottom left panel, it can be seen that MOFs with narrow pore sizes can achieve high CH_4/N_2 selectivities. For example, the most CH_4 selective (over N_2) Zr-MOF, MOF-812, has a PLD of 3.97 Å. However, it is also worthwhile to note that around the same pore size (<5 Å), several MOFs with very low CH_4/N_2 selectivities do exist (~2). This signifies that a screening purely based on PLD values to identify the selective MOFs would not necessarily lead to the highly selective materials. In contrast, those with high PLDs generally exhibit low CH_4/N_2 selectivities since the confinement effects weaken as exemplified by PCN-230 with the largest PLD size of 14.88 Å showing one of the lowest CH_4/N_2 selectivities of 1.7.

The bottom right panel describes the inverse relationship between the CH_4/N_2 selectivity and surface area of the MOFs where it is observed that the structures with large open surfaces are not very selective. Contrarily, MOFs with the

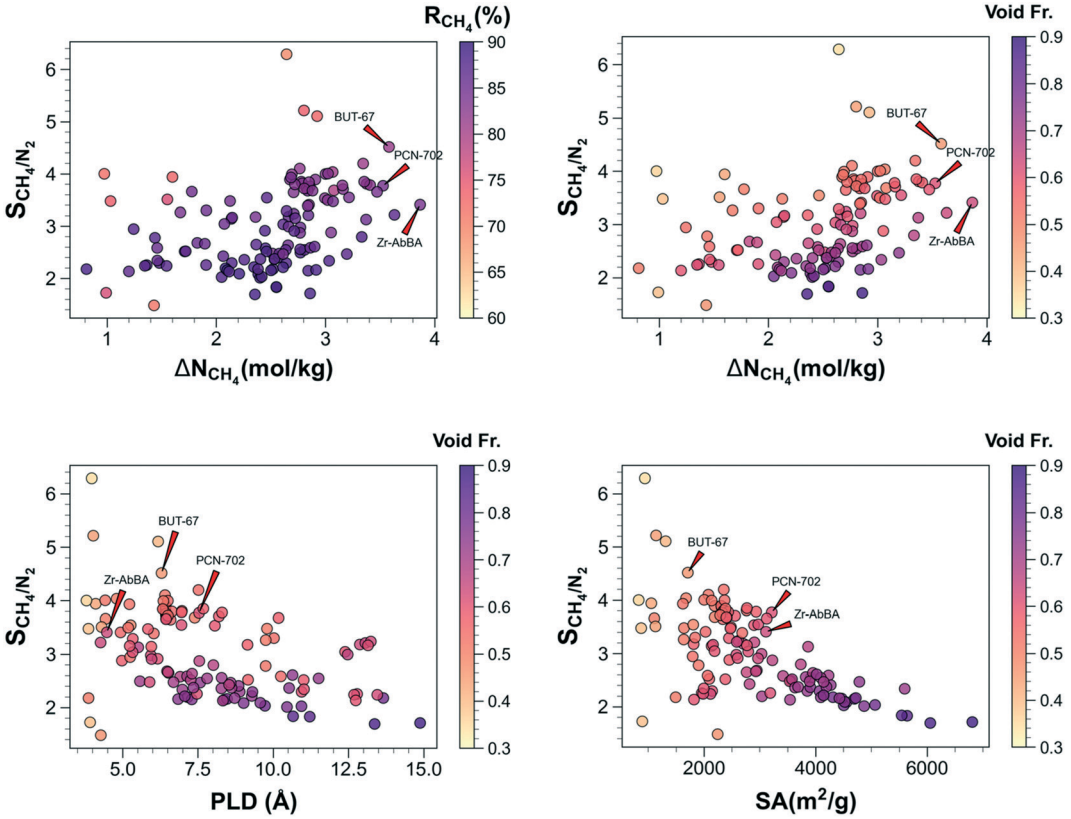

Fig. 7 CH_4/N_2 adsorption selectivities of the Zr-MOFs as a function of other two separation metrics (all calculated using PACMOF charges) and structural properties.

highest CH_4/N_2 selectivities are in the relatively low surface area region (<2000 m^2 g^{-1}). For instance, the three most selective MOFs (MOF-812, Zr-DTDC, and BUT-66) possess surface areas of 939.8, 1140.1, and 1311.7 m^2 g^{-1}. Even though there is not a linear relationship between the surface area and void fraction of the MOFs, going from left to right, it can be noticed that the void fractions tend to rise with the increase in surface areas.

The top 10 Zr-MOFs for the CH_4/N_2 separation are identified using the overall separation performance score (as calculated using PACMOF charges) and listed in Table 3 along with their separation performance metrics and structural information. These top performing MOFs with PLDs of 3.97–7.68 Å, surface areas of 939.8–3213.6 m^2 g^{-1}, and void fractions of 0.345–0.641 exhibit CH_4/N_2 selectivities of 3.2–6.3, CH_4 working capacities of 2.6–3.9 mol kg^{-1}, and CH_4 regenerabilities of 68.9–86.8%. The top three MOFs are BUT-67, Zr-AbBA, and PCN-702 showing very similar separation performances as evidenced by their similar CH_4/N_2 selectivities of 4.5, 3.4, and 3.8, CH_4 working capacities of 3.6, 3.9, and 3.5 mol kg^{-1}, and CH_4 regenerabilities of 81.1, 84.0, and 84.5%, respectively. Despite these similar metric

Table 3 Separation performance metrics calculated for the 10 top-performing Zr-MOFs (as determined using PACMOF charges) for the separation of CH_4/N_2 gas mixture

Structure	S_{CH_4/N_2}	ΔN_{CH_4} (mol kg^{-1})	R_{CH_4} (%)	GCD (Å)	PLD (Å)	LCD (Å)	SA (m^2 g^{-1})	V_f	V_p (cm^3 g^{-1})
BUT-67	4.5	3.6	81.1	7.96	6.29	7.90	1708.7	0.461	0.501
Zr-AbBA	3.4	3.9	84.0	17.87	4.48	17.87	3109.8	0.639	1.094
PCN-702	3.8	3.5	84.5	8.76	7.54	8.20	3213.6	0.612	0.813
MOF-812	6.3	2.6	68.9	5.80	3.97	5.79	939.8	0.345	0.294
PCN-700-BDC-BDDC	4.2	3.3	81.0	8.84	7.52	8.84	2353.2	0.542	0.642
MOF-525	3.2	3.6	86.8	16.27	4.27	16.27	2586.2	0.641	0.923
PCN-700-BPDC-TPDC	3.7	3.5	84.1	8.71	6.44	8.71	3122.9	0.602	0.800
LIFM-90	3.8	3.4	82.9	7.97	6.96	7.97	2933.4	0.576	0.737
PCN-700-NDC-BDDC	3.8	3.4	83.1	8.45	7.68	8.45	2768.5	0.577	0.736
LIFM-92	3.8	3.4	81.6	7.97	6.97	7.97	2761.6	0.550	0.689

GCD: global cavity diameter, PLD: pore limiting diameter, LCD: largest cavity diameter, SA: surface area, V_f: void fraction, V_p: pore volume.

values, their structural features can vary broadly considering the ranges of PLDs (4.48–7.54 Å), surface areas (1708.7–3213.6 m^2 g^{-1}), void fractions (0.461–0.639), and pore volumes (0.501–1.094 cm^3 g^{-1}).

Fig. S4† depicts the weight of each CH_4/N_2 separation performance metric on the overall separation performance score in a ternary plot. While the contributions of metrics are comparable for the top 10 materials, the contribution of the regenerability on the overall performance score can have higher impact for some of the remaining MOFs. Similar to the CF_4/CH_4 separation, this implies that neglecting regenerability may lead to a different shortlist of MOFs which could be misleading if the practical application would warrant high regenerability for cost-effectiveness. For instance, Zr-MTBC with a ranking of 22nd would rank 40th if the CH_4 regenerability was omitted. Fig. S5† portrays the CH_4 density profiles in the top three MOFs, BUT-67, Zr-AbBA, and PCN-702, identified for the CH_4/N_2 separation at the desorption and adsorption conditions. In BUT-67, CH_4 molecules prefers to adsorb near the linker, relatively close to the metal nodes creating a hexagonal adsorption pattern. In Zr-AbBA and PCN-702, CH_4 adsorbs around both the organic linker and the metal nodes where in the former, the amounts of sorbates adsorbed around these sites are comparable while in the latter, positions around the organic linkers constitute primary adsorption sites. Fig. S6† illustrates the N_2 density profiles in BUT-67, Zr-AbBA, and PCN-702, identified for the CH_4/N_2 separation at the desorption and adsorption conditions. For the N_2 adsorption sites and patterns, observations that are very similar to those for CH_4 adsorption can be made albeit some discrepancies in the relative adsorption amounts near different adsorption sites. The most notable difference is seen in PCN-702 where the adsorption amounts of N_2 molecules are comparable near both the linker and metal nodes at the adsorption conditions.

Fig. 8 delineates the normalized RDFs of the adsorbates in BUT-67, Zr-AbBA, and PCN-702 at the adsorption conditions of CH_4/N_2 mixture. As the adsorbates prefer adsorption sites near the organic linkers in BUT-67, they are located closer to the H and C atoms of the framework and O atoms of the framework are less likely to be found near the adsorbates. On the other hand, in both Zr-AbBA and PCN-702, the probability of locating O near the adsorbates, especially CH_4, is pronounced as the adsorbates adsorb near the metal nodes as well as the organic linkers. A common theme across all three materials is the presence of adsorbates in close proximity to the H and C atoms of the framework. While many commonalities can be found in the adsorption sites of the sorbates, there are also striking differences that can be exploited for the design of better performing materials. For instance, when the adsorption sites of CH_4 and N_2 in PCN-702 are contrasted in the density plots, it can be observed that the relatively weakly interacting sorbate, N_2, becomes more likely to be found around the center of the pores, where

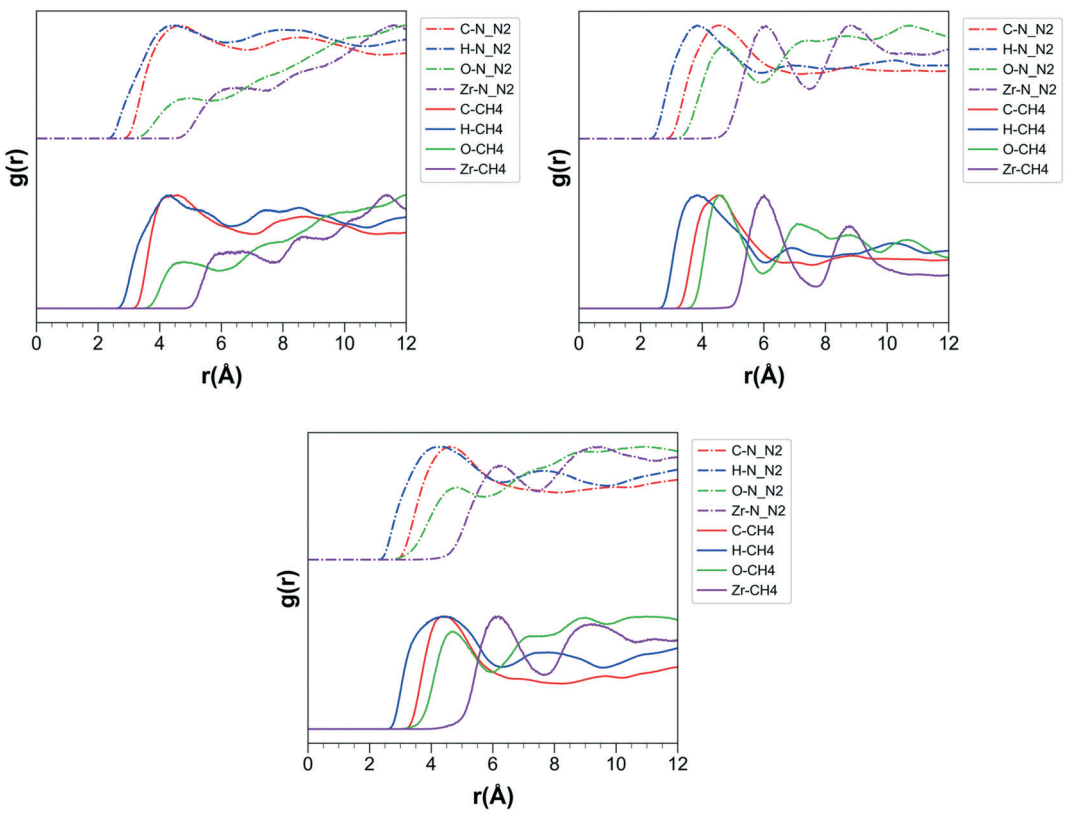

Fig. 8 Normalized RDF plots of the sorbates at 10 bar, 298 K determined for the CH_4/N_2 mixture (using PACMOF charges) in BUT-67 (left), Zr-AbBA (right), and PCN-702 (bottom).

confinement effects are less, as the pressure increases. This implies that fragmenting such large pores into smaller pores can boost the confinement effect for the strongly interacting sorbate, CH_4, which would potentially cause CH_4/N_2 selectivity to be even higher in addition to expanding CH_4 working capacity and regenerability.

One question that generally arises in the screening studies is whether the method of assigning atomic charges may significantly influence the gas separation performances. Indeed, the different methods of assigning partial charges to the framework atoms can lead to significantly disparate predictions of gas adsorption and/or separation performance as shown earlier.[77–79] Here, we initially employed PACMOF charges to predict the CH_4/N_2 separation performances of Zr-MOFs as they can be of a quality comparable to DDEC charges.[59] To investigate the influence of the atomic charges on the calculated gas separation performance metrics and overall material rankings, the GCMC calculations are repeated with EQeq charges for the separation of the CH_4/N_2 mixture from which gas separation performance metrics and material rankings are determined. To the best of our knowledge, this is the first study investigating MOFs' CH_4/N_2 separation performance using PACMOF charges and comparing CH_4/N_2 separation performance predictions based on PACMOF and EQeq charges. Fig. 9 compares the MOF rankings, CH_4/N_2 selectivities, CH_4 working capacities, and regenerabilities acquired using PACMOF and EQeq charges. It can be seen that the deviations in CH_4 working capacities and regenerabilities are insignificant. While Kancharlapalli *et al.*[59] demonstrated earlier that the gas selectivities (*i.e.*, CO_2/N_2) can differ a lot using PACMOF and EQeq charges for some MOFs, it has been observed here that these different charge assignment methods did not lead to drastically different CH_4/N_2 selectivities for almost all MOFs except one case (*i.e.*, PCN-59 attaining CH_4/N_2 selectivities of 1.5 and 3.8 using PACMOF and EQeq charges, respectively). This can be attributed to the presence of only one adsorbate with partial charges and its relatively weak interaction with the framework (compared to CH_4) limiting the effect of charges on the CH_4/N_2 separation performances of the MOFs. As these three gas separation performance metrics directly influence the material rankings, there are some discrepancies in the MOF rankings determined using PACMOF and EQeq charges. However, these discrepancies are in limited extent and the majority of the points lie on the parity line. The biggest discrepancy in the rankings is observed for BUT-10 ranking 46th and 22nd based on PACMOF and EQeq charges, respectively. Among the top 10 materials identified using PACMOF charges, 8 materials exist in the top 10 performing material list based on EQeq charges. Overall, these observations imply that PACMOF and EQeq charges provide very similar results. This observation corroborates with the presence of highly correlated MOF rankings for CO_2/CH_4 separation as obtained through Qeq (charge equilibration)[80]

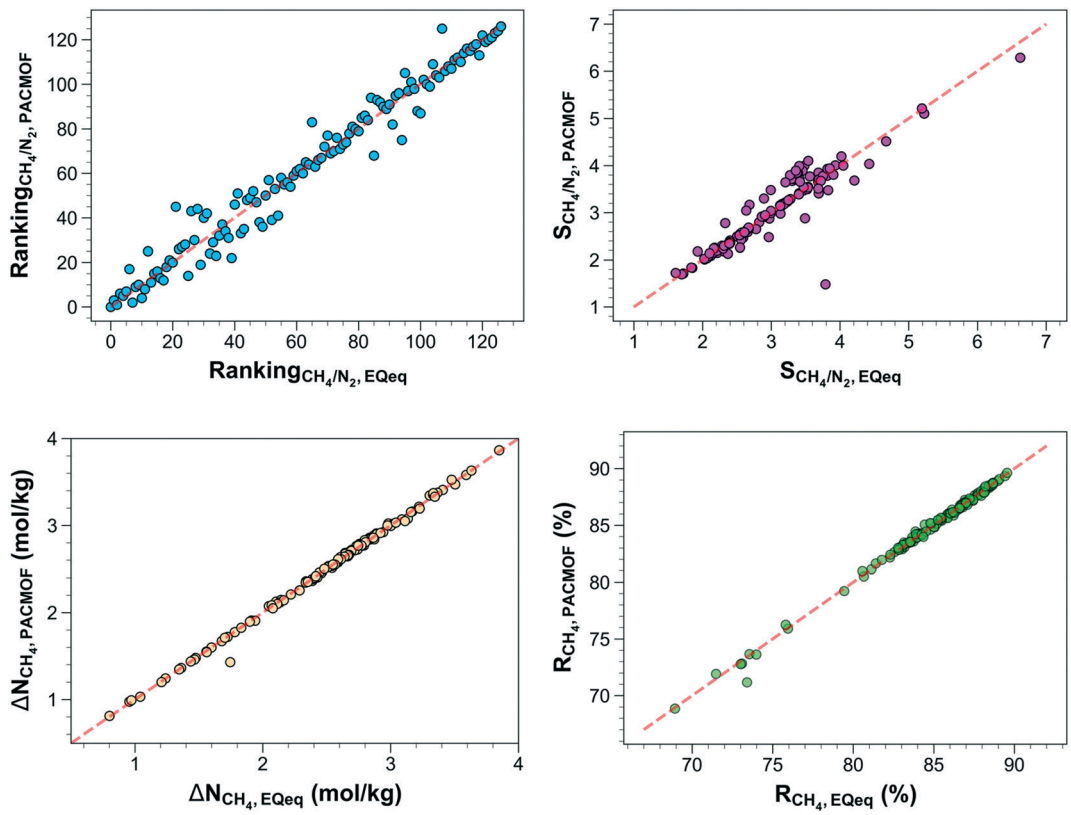

Fig. 9 Comparison of material rankings, CH_4/N_2 selectivities, CH_4 working capacities, and CH_4 regenerabilities obtained for the separation of CH_4/N_2 gas mixture using PACMOF and EQeq charges. (Dashed line represents parity line).

and DDEC (density-derived electrostatic and chemical charge method)[81] charges in a recent work.[77] However, it should be noted that the results obtained by the two charge methods used in this study may not necessarily be alike for other gas separation applications or MOF lists.

In the literature, there are not many CF_4/CH_4 separation studies reporting selectivities. One of the rare studies reporting CF_4/CH_4 selectivity is by Buss *et al.*[82] which experimentally determined CF_4/CH_4 selectivity of silicalite to be around 2.25 for an equimolar mixture at 17 bar, 298.15 K. As the adsorption pressure in this study is much lower, a direct comparison is not possible. However, it can be expected that many of the MOFs that show CF_4/CH_4 selectivities around 2 or higher could outperform silicalite at the ambient conditions since we generally observed higher CF_4/CH_4 selectivities as the pressure is lowered (0.7–11.9). Another study on silicalite was published by Heuchel *et al.*[83] where the CF_4/CH_4 selectivity for an equimolar mixture at 1 bar, 300 K is determined about 4.5 using GCMC simulations. In this work, six Zr-MOFs (BUT-66, PU-1, PCN-700-BPDC-TPDC, BUT-67, LIFM-90, and BUT-11) are found to outperform this separation performance. The CH_4/H_2 and CH_4/N_2 selectivities calculated in this study are mostly in the vicinity of the reported values in the literature,[46,48,50,52] yet, a full comparison of three performance metrics is not generally possible as they are not available for many materials studied previously. However, many of the Zr-MOFs investigated in this work are more selective than conventional adsorbents. For instance, Li *et al.*[84] demonstrated that the activated carbon is almost unselective for an equimolar CH_4/N_2 mixture at room temperature, 10 bar. Likewise, Krishna *et al.*[85] determined CH_4/H_2 selectivities (<15) of several zeolites (CHA, ITQ-29, LTA-Si) around room temperature, 10 bar which can be superseded by many of the MOFs studied herein.

Having identified the best materials for the separations of CF_4/CH_4, CH_4/H_2, and CH_4/N_2 mixtures, now we turn to the subject of water stability of Zr-MOFs as the gas adsorption conditions could be humid affecting the structural stability and/or gas separation performances. Fig. S7† depicts the Henry's constants (K_{H,H_2O}) and heats of adsorption of H_2O ($-\Delta H°_{H_2O}$) at infinite dilution in Zr-MOFs at 298 K which span the ranges of $1.5 \times 10^{-6} - 2.2 \times 10^{16}$ mmol g^{-1} Pa^{-1} and 9.4–159.5 kJ mol^{-1}. K_{H,H_2O} and $-\Delta H°_{H_2O}$ values are determined for 9 out of the top 10 materials identified for the CF_4/CH_4, CH_4/H_2, and CH_4/N_2 separation with reasonable accuracy (<50% deviation for K_{H,H_2O}). These values extend in the ranges of $1.2 \times 10^{-5} - 2.6 \times 10^{-1}$ mmol g^{-1} Pa^{-1} and 21.0–61.1 kJ mol^{-1}, $3.1 \times 10^{-6} - 2.6 \times 10^{-1}$ mmol g^{-1} Pa^{-1} and 14.7–61.1 kJ mol^{-1}, and $1.4 \times 10^{-4} - 2.6 \times 10^{-1}$ mmol g^{-1} Pa^{-1} and 35.5–61.1 kJ mol^{-1}, respectively. Earlier, it is suggested by Moghadam *et al.*[86] that the structures having $K_{H,H_2O} < 5 \times 10^{-6}$ mmol g^{-1} Pa^{-1} could be considered hydrophobic considering ZIF-8 as a reference. Among the top 10 materials identified for each gas separation, based on this preliminary analysis, Zr-DTDC appearing in the top 10 materials for the CH_4/H_2 separation is computed to have K_{H,H_2O} of 3×10^{-6} mmol g^{-1} Pa^{-1} and $-\Delta H°_{H_2O}$ of 14.7 kJ mol^{-1} which can be deemed as hydrophobic implying that it has potential for practical use due to limited water affinity. To sum up, our computational analysis identifies the most promising materials for the CF_4/CH_4, CH_4/H_2, and CH_4/N_2 separations and provides molecular-level insights into the preferred adsorption sites for both sorbates in the mixtures. As the water stability of MOFs is crucial in determining their final use in applications, MOFs' water affinities are computed among which those with lower water affinities would be more preferable for practical use. However, this does not necessarily mean that MOFs with moderate/high water affinities would always be impractical as they may remain stable even in the presence of water.

It is known that the flexibility of the structures can ease the diffusion of gas molecules into the pores and, in some cases, improve gas storage/separation performances of MOF adsorbents and membranes.[87–89] For instance, Witman *et al.*'s theoretical analysis[89] demonstrated that a judiciously designed flexible material can outperform the CH_4 delivery performance of rigid materials. Thus, ideally, MOFs should be modeled flexible. However, as the objective of this work is to screen a large number of MOFs and identify the potentially useful ones for the foregoing gas separations at a viable computational cost, the flexibility effects are not considered.

Besides material properties and performances, another important factor in deciding the material to use in practical applications is process economics. It has been shown earlier that material separation performances and process level objectives do not necessarily correlate well with each other.[90,91] Therefore, as a further evaluation, practical metrics such as purity, recovery, and capture cost should be considered to holistically understand the potential benefits of the materials discussed herein. Recently, Danaci *et al.*[92] revealed the correlations between various structural features, adsorption amounts of weakly interacting gas (*i.e.*, N_2) and purity levels of strongly interacting gas (*i.e.*, CO_2) in their work bridging molecular modeling to process modeling.

Last but not the least, while it is not within the scope of this work, it should be noted that the identification of the MOFs with favorable and targeted adsorption characteristics may not only help foster advancements in the field of gas separation but also catalysis as the captured sorbates can be transformed into valuable products on the same MOF as shown by Muller *et al.*[93] for CO_2 adsorption and conversion. We hope that our computational work narrowing down promising materials for CF_4/CH_4, CH_4/H_2, and CH_4/N_2 separations will guide further experimental and theoretical works.

4. Conclusions

To conclude, our computational screening work identifies the most promising Zr-MOFs among a list of >100 Zr-MOFs reported earlier for the separation of equimolar CF_4/CH_4,

CH_4/H_2, and CH_4/N_2 mixtures at room temperature. As the selected Zr-MOFs do not include open metal sites, our generic force field-based predictions do not suffer from the deficiency of accurate representation of interactions between the open metal sites and the adsorbates. While the open metal sites can interact strongly with sorbates potentially leading to high selectivities (*e.g.*, CH_4/N_2 selectivity of 9.7 acquired by ATC-Cu (ref. 94)), our choice of eliminating MOFs with open metal sites avoids having potentially inaccurate predictions due to known drawbacks of generic force fields. It should be noted that the presence of open metal sites does not necessarily mean high gas selectivity as exemplified by HKUST-1 attaining a relatively low CH_4/N_2 selectivity of 3.7 (ref. 94) which is lower than the predicted selectivities of many Zr-MOFs studied in this work. This is not surprising as there are multiple factors influencing the gas selectivities such as pore size, shape, functional groups, *etc.* In addition, as the foregoing discussions point out, the adsorption selectivity is not the only metric determining the material rankings as the separation economics rely on multiple factors including working capacity and regenerability. Therefore, while there can be more selective MOFs with open metal sites than the ones identified in this work, they may exhibit limited working capacity and/or regenerability as they can have relatively low pore volumes and incomplete activation as a result of very strong interactions hampering overall gas separation performance.[95,96] The overly strong interactions can cause MOFs to experience high levels of strain and even degrade during regeneration owing to high level of heating needed for their reuse.[97,98] Considering these multiple factors, a more selective MOF with open metal sites may still perform worse than a less selective MOF without open metal site in a real gas separation process.

Herein, the top performing materials are ranked by considering all three performance metrics calculated; adsorption selectivity, working capacity, and regenerability. For the CF_4/CH_4 separation, PCN-700-BPDC-TPDC, LIFM-90, and BUT-67 are evaluated to be the best three materials with CF_4/CH_4 adsorption selectivities of 4.8, 4.6, and 4.7, CF_4 working capacities of 2.0, 2.0, and 2.1 mol kg^{-1}, and CF_4 regenerabilities of 85.1, 84.2, and 75.7%, respectively. For the CH_4/H_2 separation, MOF-812, BUT-67, and BUT-66 rank as the top three MOFs having CH_4/H_2 selectivities of 61.6, 36.7, and 46.2, CH_4 working capacities of 3.0, 4.1, and 3.4 mol kg^{-1}, and CH_4 regenerabilities of 70.7, 82.7, and 74.7%, in successive order. Our investigation revealed the three top-performing MOFs for the CH_4/N_2 separation as BUT-67, Zr-AbBA, and PCN-702 attaining CH_4/N_2 selectivities of 4.5, 3.4, and 3.8, CH_4 working capacities of 3.6, 3.9, and 3.5 mol kg^{-1}, and CH_4 regenerabilities of 81.1, 84.0, and 84.5%, successively. In these materials, sorbates are found to be located closest to the H and C atoms of the framework. In general, the most selective MOFs lie in the small PLD region, however, they do not necessarily turn out to be the best materials overall as there is an interplay of several factors in determining the overall separation performance. The identified top performing materials generally have relatively narrow PLDs of $\sim$ 4–8 Å, low to medium surface areas of $\sim$ 1000–3000 m^2 g^{-1}, and medium-high void fractions of $\sim$ 0.35–0.65.

Conflicts of interest

The authors declare no competing financial interest.

Acknowledgements

S. K. acknowledges ERC-2017-Starting Grant. This study has received funding from the European Research Council (ERC) under the European Union's Horizon 2020 research and innovation programme (ERC-2017-Starting Grant, grant agreement no. 756489-COSMOS). The numerical calculations reported in this paper were partially performed at TUBITAK ULAKBIM, High Performance and Grid Computing Center (TRUBA resources).

References

1 Y. Chen, X. Zhang, M. R. Mian, F. A. Son, K. Zhang, R. Cao, Z. Chen, S.-J. Lee, K. B. Idrees, T. A. Goetjen, J. Lyu, P. Li, Q. Xia, Z. Li, J. T. Hupp, T. Islamoglu, A. Napolitano, G. W. Peterson and O. K. Farha, *J. Am. Chem. Soc.*, 2020, **142**, 21428–21438.
2 S. E. Bambalaza, H. W. Langmi, R. Mokaya, N. M. Musyoka, J. Ren and L. E. Khotseng, *J. Mater. Chem. A*, 2018, **6**, 23569–23577.
3 Z. Lu, J. Liu, X. Zhang, Y. Liao, R. Wang, K. Zhang, J. Lyu, O. K. Farha and J. T. Hupp, *J. Am. Chem. Soc.*, 2020, **142**, 21110–21121.
4 Z. Hu, Y. Wang and D. Zhao, *Chem. Soc. Rev.*, 2021, **50**, 4629–4683.
5 B. Ye, A. Gheorghe, R. van Hal, M. Zevenbergen and S. Tanase, *Mol. Syst. Des. Eng.*, 2020, **5**, 1071–1076.
6 N. Panagiotou, K. Evangelou, A. Psalti, N. Varnava, G. K. Angeli, P. N. Trikalitis, J. C. Plakatouras, T. Lazarides and A. J. Tasiopoulos, *Mol. Syst. Des. Eng.*, 2020, **5**, 1077–1087.
7 Y. Lin, C. Kong, Q. Zhang and L. Chen, *Adv. Energy Mater.*, 2017, **7**, 1601296.
8 K. Sumida, D. L. Rogow, J. A. Mason, T. M. McDonald, E. D. Bloch, Z. R. Herm, T.-H. Bae and J. R. Long, *Chem. Rev.*, 2012, **112**, 724–781.
9 J.-R. Li, R. J. Kuppler and H.-C. Zhou, *Chem. Soc. Rev.*, 2009, **38**, 1477–1504.
10 X. Sun, X. Li, S. Yao, R. Krishna, J. Gu, G. Li and Y. Liu, *J. Mater. Chem. A*, 2020, **8**, 17106–17112.
11 I. Abánades Lázaro, C. J. R. Wells and R. S. Forgan, *Angew. Chem., Int. Ed.*, 2020, **59**, 5211–5217.
12 M. Rimoldi, A. J. Howarth, M. R. DeStefano, L. Lin, S. Goswami, P. Li, J. T. Hupp and O. K. Farha, *ACS Catal.*, 2017, **7**, 997–1014.
13 T. N. Tu, M. V. Nguyen, H. L. Nguyen, B. Yuliarto, K. E. Cordova and S. Demir, *Coord. Chem. Rev.*, 2018, **364**, 33–50.

14 X. Liu, K. O. Kirlikovali, Z. Chen, K. Ma, K. B. Idrees, R. Cao, X. Zhang, T. Islamoglu, Y. Liu and O. K. Farha, *Chem. Mater.*, 2021, **33**, 1444–1454.
15 J. F. Kurisingal, Y. Rachuri, A. S. Palakkal, R. S. Pillai, Y. Gu, Y. Choe and D.-W. Park, *ACS Appl. Mater. Interfaces*, 2019, **11**, 41458–41471.
16 T. C. Wang, W. Bury, D. A. Gómez-Gualdrón, N. A. Vermeulen, J. E. Mondloch, P. Deria, K. Zhang, P. Z. Moghadam, A. A. Sarjeant, R. Q. Snurr, J. F. Stoddart, J. T. Hupp and O. K. Farha, *J. Am. Chem. Soc.*, 2015, **137**, 3585–3591.
17 K. B. Idrees, Z. Chen, X. Zhang, M. R. Mian, R. J. Drout, T. Islamoglu and O. K. Farha, *Chem. Mater.*, 2020, **32**, 3776–3782.
18 L.-M. Yang, E. Ganz, S. Svelle and M. Tilset, *J. Mater. Chem. C*, 2014, **2**, 7111–7125.
19 A. J. Howarth, Y. Liu, P. Li, Z. Li, T. C. Wang, J. T. Hupp and O. K. Farha, *Nat. Rev. Mater.*, 2016, **1**, 15018.
20 D. Feng, Z.-Y. Gu, J.-R. Li, H.-L. Jiang, Z. Wei and H.-C. Zhou, *Angew. Chem., Int. Ed.*, 2012, **51**, 10307–10310.
21 T.-F. Liu, D. Feng, Y.-P. Chen, L. Zou, M. Bosch, S. Yuan, Z. Wei, S. Fordham, K. Wang and H.-C. Zhou, *J. Am. Chem. Soc.*, 2015, **137**, 413–419.
22 H. Furukawa, F. Gándara, Y.-B. Zhang, J. Jiang, W. L. Queen, M. R. Hudson and O. M. Yaghi, *J. Am. Chem. Soc.*, 2014, **136**, 4369–4381.
23 T. Matemb Ma Ntep, H. Breitzke, L. Schmolke, C. Schlüsener, B. Moll, S. Millan, N. Tannert, I. El Aita, G. Buntkowsky and C. Janiak, *Chem. Mater.*, 2019, **31**, 8629–8638.
24 Z. Hu, Y. Wang, S. Farooq and D. Zhao, *AIChE J.*, 2017, **63**, 4103–4114.
25 D. Feng, Z.-Y. Gu, Y.-P. Chen, J. Park, Z. Wei, Y. Sun, M. Bosch, S. Yuan and H.-C. Zhou, *J. Am. Chem. Soc.*, 2014, **136**, 17714–17717.
26 S. Wang, J. Wang, W. Cheng, X. Yang, Z. Zhang, Y. Xu, H. Liu, Y. Wu and M. Fang, *Dalton Trans.*, 2015, **44**, 8049–8061.
27 S. Yuan, J.-S. Qin, C. T. Lollar and H.-C. Zhou, *ACS Cent. Sci.*, 2018, **4**, 440–450.
28 R. L. Siegelman, P. J. Milner, A. C. Forse, J.-H. Lee, K. A. Colwell, J. B. Neaton, J. A. Reimer, S. C. Weston and J. R. Long, *J. Am. Chem. Soc.*, 2019, **141**, 13171–13186.
29 B. Wang, L.-H. Xie, X. Wang, X.-M. Liu, J. Li and J.-R. Li, *Green Energy Environ.*, 2018, **3**, 191–228.
30 Z. R. Herm, E. D. Bloch and J. R. Long, *Chem. Mater.*, 2014, **26**, 323–338.
31 H. Daglar, H. C. Gulbalkan, G. Avci, G. O. Aksu, O. F. Altundal, C. Altintas, I. Erucar and S. Keskin, *Angew. Chem., Int. Ed.*, 2021, **60**, 7828–7837.
32 J. Rogacka, A. Seremak, A. Luna-Triguero, F. Formalik, I. Matito-Martos, L. Firlej, S. Calero and B. Kuchta, *Chem. Eng. J.*, 2021, **403**, 126392.
33 S. M. Miller, S. C. Wofsy, A. M. Michalak, E. A. Kort, A. E. Andrews, S. C. Biraud, E. J. Dlugokencky, J. Eluszkiewicz, M. L. Fischer, G. Janssens-Maenhout, B. R. Miller, J. B. Miller, S. A. Montzka, T. Nehrkorn and C. Sweeney, *Proc. Natl. Acad. Sci. U. S. A.*, 2013, **110**, 20018–20022.
34 P. Kowalczyk and R. Holyst, *Environ. Sci. Technol.*, 2008, **42**, 2931–2936.
35 R. K. Motkuri, H. V. R. Annapureddy, M. Vijaykumar, H. T. Schaef, P. F. Martin, B. P. McGrail, L. X. Dang, R. Krishna and P. K. Thallapally, *Nat. Commun.*, 2014, **5**, 4368.
36 I. Senkovska, E. Barea, J. A. R. Navarro and S. Kaskel, *Microporous Mesoporous Mater.*, 2012, **156**, 115–120.
37 A. Alonso, J. Moral-Vico, A. Abo Markeb, M. Busquets-Fité, D. Komilis, V. Puntes, A. Sánchez and X. Font, *Sci. Total Environ.*, 2017, **595**, 51–62.
38 S. W. Choi, D.-H. Lee, J. Kim, J. Kim, J.-H. Park, H. T. Beum, D.-S. Lim and K. B. Lee, *Chem. Eng. J.*, 2017, **311**, 227–235.
39 N.-G. Ahn, S.-W. Kang, B.-H. Min and S.-S. Suh, *J. Chem. Eng. Data*, 2006, **51**, 451–456.
40 M.-Q. Liu, C. Wang, Z. Yao and N.-Y. Kim, *RSC Adv.*, 2016, **6**, 41580–41586.
41 P. Balcombe, J. F. Speirs, N. P. Brandon and A. D. Hawkes, *Environ. Sci.: Processes Impacts*, 2018, **20**, 1323–1339.
42 P. Schwach, X. Pan and X. Bao, *Chem. Rev.*, 2017, **117**, 8497–8520.
43 C. L. Weber and C. Clavin, *Environ. Sci. Technol.*, 2012, **46**, 5688–5695.
44 S. Calero, J. J. Gutiérrez-Sevillano and E. García-Pérez, *Microporous Mesoporous Mater.*, 2013, **165**, 79–83.
45 M. Gallo and D. Glossman-Mitnik, *J. Phys. Chem. C*, 2009, **113**, 6634–6642.
46 D. Wu, C. Wang, B. Liu, D. Liu, Q. Yang and C. Zhong, *AIChE J.*, 2012, **58**, 2078–2084.
47 H. Guo, F. Shi, Z. Ma and X. Liu, *J. Phys. Chem. C*, 2010, **114**, 12158–12165.
48 C. Altintas, G. Avci, H. Daglar, A. N. V. Azar, I. Erucar, S. Velioglu and S. Keskin, *J. Mater. Chem. A*, 2019, **7**, 9593–9608.
49 C. Altintas, G. Avci, H. Daglar, E. Gulcay, I. Erucar and S. Keskin, *J. Mater. Chem. A*, 2018, **6**, 5836–5847.
50 B. Liu, Q. Yang, C. Xue, C. Zhong, B. Chen and B. Smit, *J. Phys. Chem. C*, 2008, **112**, 9854–9860.
51 S. U. Nandanwar, D. R. Corbin and M. B. Shiflett, *Ind. Eng. Chem. Res.*, 2020, **59**, 13355–13369.
52 Z. Sumer and S. Keskin, *Ind. Eng. Chem. Res.*, 2017, **56**, 8713–8722.
53 C. E. Kivi, B. S. Gelfand, H. Dureckova, H. T. K. Ho, C. Ma, G. K. H. Shimizu, T. K. Woo and D. Song, *Chem. Commun.*, 2018, **54**, 14104–14107.
54 L. Li, L. Yang, J. Wang, Z. Zhang, Q. Yang, Y. Yang, Q. Ren and Z. Bao, *AIChE J.*, 2018, **64**, 3681–3689.
55 A. L. Myers and J. M. Prausnitz, *AIChE J.*, 1965, **11**, 121–127.
56 Z. Qiao, C. Peng, J. Zhou and J. Jiang, *J. Mater. Chem. A*, 2016, **4**, 15904–15912.
57 T.-H. Kim, S.-Y. Kim, T.-U. Yoon, M.-B. Kim, W. Park, H. H. Han, C. Kong, C.-Y. Park, J.-H. Kim and Y.-S. Bae, *Chem. Eng. J.*, 2020, **399**, 125717.
58 X.-W. Liu, Y.-M. Gu, T.-J. Sun, Y. Guo, X.-L. Wei, S.-S. Zhao and S.-D. Wang, *Ind. Eng. Chem. Res.*, 2019, **58**, 20392–20400.
59 S. Kancharlapalli, A. Gopalan, M. Haranczyk and R. Q. Snurr, *J. Chem. Theory Comput.*, 2021, **17**(5), 3052–3064.

60 C. E. Wilmer, K. C. Kim and R. Q. Snurr, *J. Phys. Chem. Lett.*, 2012, **3**, 2506–2511.
61 F. Zhou, B. Zheng, D. Liu, Z. Wang and Q. Yang, *ACS Appl. Mater. Interfaces*, 2019, **11**, 46984–46992.
62 D. Dubbeldam, S. Calero, D. E. Ellis and R. Q. Snurr, *Mol. Simul.*, 2016, **42**, 81–101.
63 A. I. Skoulidas, T. C. Bowen, C. M. Doelling, J. L. Falconer, R. D. Noble and D. S. Sholl, *J. Membr. Sci.*, 2003, **227**, 123–136.
64 M. G. Martin and J. I. Siepmann, *J. Phys. Chem. B*, 1998, **102**, 2569–2577.
65 J. J. Potoff and J. I. Siepmann, *AIChE J.*, 2001, **47**, 1676–1682.
66 V. Buch, *J. Chem. Phys.*, 1994, **100**, 7610–7629.
67 A. K. Rappe, C. J. Casewit, K. S. Colwell, W. A. Goddard and W. M. Skiff, *J. Am. Chem. Soc.*, 1992, **114**, 10024–10035.
68 P. P. Ewald, *Ann. Phys.*, 1921, **64**, 253–287.
69 T. F. Willems, C. H. Rycroft, M. Kazi, J. C. Meza and M. Haranczyk, *Microporous Mesoporous Mater.*, 2012, **149**, 134–141.
70 M. J. Lennox, M. Bound, A. Henley and E. Besley, *Mol. Simul.*, 2017, **43**, 828–837.
71 J. G. McDaniel, S. Li, E. Tylianakis, R. Q. Snurr and J. R. Schmidt, *J. Phys. Chem. C*, 2015, **119**, 3143–3152.
72 P. Z. Moghadam, T. Islamoglu, S. Goswami, J. Exley, M. Fantham, C. F. Kaminski, R. Q. Snurr, O. K. Farha and D. Fairen-Jimenez, *Nat. Commun.*, 2018, **9**, 1378.
73 S. M. McIntyre, B. Shan, R. Wang, C. Zhong, J. Liu and B. Mu, *Ind. Eng. Chem. Res.*, 2018, **57**, 9240–9253.
74 Q. Yang, A. D. Wiersum, P. L. Llewellyn, V. Guillerm, C. Serre and G. Maurin, *Chem. Commun.*, 2011, **47**, 9603–9605.
75 A. L. Spek, *J. Appl. Crystallogr.*, 2003, **36**, 7–13.
76 A. L. Spek, *Acta Crystallogr., Sect. D: Biol. Crystallogr.*, 2009, **65**, 148–155.
77 C. Altintas and S. Keskin, *Mol. Syst. Des. Eng.*, 2020, **5**, 532–543.
78 K. Sladekova, C. Campbell, C. Grant, A. J. Fletcher, J. R. B. Gomes and M. Jorge, *Adsorption*, 2020, **26**, 663–685.
79 D. Ongari, P. G. Boyd, O. Kadioglu, A. K. Mace, S. Keskin and B. Smit, *J. Chem. Theory Comput.*, 2019, **15**, 382–401.
80 A. K. Rappe and W. A. Goddard, *J. Phys. Chem.*, 1991, **95**, 3358–3363.
81 T. A. Manz and D. S. Sholl, *J. Chem. Theory Comput.*, 2010, **6**, 2455–2468.
82 E. Buss and M. Heuchel, *J. Chem. Soc., Faraday Trans.*, 1997, **93**, 1621–1628.
83 M. Heuchel, R. Q. Snurr and E. Buss, *Langmuir*, 1997, **13**, 6795–6804.
84 L. Li, J. Yang, J. Li, Y. Chen and J. Li, *Microporous Mesoporous Mater.*, 2014, **198**, 236–246.
85 R. Krishna and J. M. van Baten, *Phys. Chem. Chem. Phys.*, 2011, **13**, 10593–10616.
86 P. Z. Moghadam, D. Fairen-Jimenez and R. Q. Snurr, *J. Mater. Chem. A*, 2016, **4**, 529–536.
87 N. Chanut, A. Ghoufi, M.-V. Coulet, S. Bourrelly, B. Kuchta, G. Maurin and P. L. Llewellyn, *Nat. Commun.*, 2020, **11**, 1216.
88 S. Hiraide, Y. Sakanaka, H. Kajiro, S. Kawaguchi, M. T. Miyahara and H. Tanaka, *Nat. Commun.*, 2020, **11**, 3867.
89 M. Witman, S. Ling, V. Stavila, P. Wijeratne, H. Furukawa and M. D. Allendorf, *Mol. Syst. Des. Eng.*, 2020, **5**, 1491–1503.
90 J. Park, H. O. Rubiera Landa, Y. Kawajiri, M. J. Realff, R. P. Lively and D. S. Sholl, *Ind. Eng. Chem. Res.*, 2020, **59**, 7097–7108.
91 D. Yancy-Caballero, K. T. Leperi, B. J. Bucior, R. K. Richardson, T. Islamoglu, O. K. Farha, F. You and R. Q. Snurr, *Mol. Syst. Des. Eng.*, 2020, **5**, 1205–1218.
92 D. Danaci, M. Bui, N. Mac Dowell and C. Petit, *Mol. Syst. Des. Eng.*, 2020, **5**, 212–231.
93 P. Müller, B. Bucior, G. Tuci, L. Luconi, J. Getzschmann, S. Kaskel, R. Q. Snurr, G. Giambastiani and A. Rossin, *Mol. Syst. Des. Eng.*, 2019, **4**, 1000–1013.
94 Z. Niu, X. Cui, T. Pham, P. C. Lan, H. Xing, K. A. Forrest, L. Wojtas, B. Space and S. Ma, *Angew. Chem., Int. Ed.*, 2019, **58**, 10138–10141.
95 S. Ye, X. Jiang, L.-W. Ruan, B. Liu, Y.-M. Wang, J.-F. Zhu and L.-G. Qiu, *Microporous Mesoporous Mater.*, 2013, **179**, 191–197.
96 C. A. Trickett, A. Helal, B. A. Al-Maythalony, Z. H. Yamani, K. E. Cordova and O. M. Yaghi, *Nat. Rev. Mater.*, 2017, **2**, 17045.
97 P. Kumar, B. Anand, Y. F. Tsang, K.-H. Kim, S. Khullar and B. Wang, *Environ. Res.*, 2019, **176**, 108488.
98 Q.-G. Zhai, X. Bu, C. Mao, X. Zhao, L. Daemen, Y. Cheng, A. J. Ramirez-Cuesta and P. Feng, *Nat. Commun.*, 2016, **7**, 13645.